Journal of
Composites Science

MDPI

Article

Spark Plasma Sintering and Hot Pressing of Cu+Al Powder Mixtures and Pre-Deposited Cu/Al Layers

Dina V. Dudina [1,2,*], Boris B. Bokhonov [2], Alexander I. Gavrilov [2], Vladimir Yu. Ulianitsky [1], Arina V. Ukhina [2], Aigul A. Ondar [2,3], Serguei F. Tikhov [4] and Oleg L. Smorygo [5,6]

1 Lavrentyev Institute of Hydrodynamics SB RAS, Lavrentyev Ave. 15, 630090 Novosibirsk, Russia; ulianv@mail.ru
2 Institute of Solid State Chemistry and Mechanochemistry SB RAS, Kutateladze Str. 18, 630090 Novosibirsk, Russia; bokhonov@solid.nsc.ru (B.B.B.); gavr_sand@mail.ru (A.I.G.); auhina181@gmail.com (A.V.U.); aigulondar2199@mail.ru (A.A.O.)
3 Department of Natural Sciences, Novosibirsk State University, Pirogova Str. 1, 630090 Novosibirsk, Russia
4 Boreskov Institute of Catalysis SB RAS, Lavrentyev Ave. 5, 630090 Novosibirsk, Russia; tikhov@catalysis.ru
5 UTS Synthesis Ltd., UTS Group, Begomlskaya Str. 23, 220053 Minsk, Belarus; olegsmorygo@yahoo.com
6 O.V. Roman Powder Metallurgy Institute, National Academy of Sciences of Belarus, Platonov Str. 41, 220005 Minsk, Belarus
* Correspondence: dina1807@gmail.com

Abstract: Reactive processing of metals is interesting for materials design and achieving new sets of properties. The transformation degree of the metals, the factor governing the properties of the material as a whole, depends on the sintering/heat treatment conditions. In the present investigation, the phase and microstructure formation of materials obtained by sintering of Cu-10 wt.% Al mixtures and layered Cu/Al structures under different modes of pressing/heating is presented. The samples were obtained via spark plasma sintering (SPS), hot pressing (HP) and pressureless sintering. The products of the interaction between the metals were Al_2Cu and Cu_9Al_4 intermetallics and Cu(Al) solid solutions. The influence of the consolidation method on the phase composition of the sintered materials was studied. The hardness of the composites was analyzed in relation to their structural features. A model experiment has been conducted to trace the structural evolution at the Cu/Al interface caused by interdiffusion. The Cu/Al layered structures obtained by detonation spraying of the powders on a steel substrate were treated by SPS or HP. The effect of electric current, which is a feature of SPS processing, was in accelerating the reaction product formation in the layered structures still containing the starting metallic reactants.

Keywords: spark plasma sintering; hot pressing; copper; aluminum; composite; intermetallic; hardness; microstructure; diffusion

check for updates

Citation: Dudina, D.V.; Bokhonov, B.B.; Gavrilov, A.I.; Ulianitsky, V.Y.; Ukhina, A.V.; Ondar, A.A.; Tikhov, S.F.; Smorygo, O.L. Spark Plasma Sintering and Hot Pressing of Cu+Al Powder Mixtures and Pre-Deposited Cu/Al Layers. *J. Compos. Sci.* **2023**, *7*, 466. https://doi.org/10.3390/jcs7110466

Academic Editor: Prashanth Konda Gokuldoss

Received: 13 September 2023
Revised: 20 October 2023
Accepted: 3 November 2023
Published: 7 November 2023

Copyright: © 2023 by the authors. Licensee MDPI, Basel, Switzerland. This article is an open access article distributed under the terms and conditions of the Creative Commons Attribution (CC BY) license (https://creativecommons.org/licenses/by/4.0/).

1. Introduction

Materials formed via reactions between metals are interesting from the viewpoint of achieving new sets of mechanical and functional properties [1–4]. The binary Cu-Al system is the basis for the fabrication of Al-based alloys [5,6], aluminum bronzes [7–11] as well as composite structures and joints [12–21]. In bronzes, a higher mechanical strength and a better corrosion resistance than those of pure copper are sought. The Cu-Al composites and joined (welded) assemblies find applications in electrical and electronic engineering.

Cu/Al structures have been obtained by high-pressure torsion/annealing [13], rolling/annealing [17], solid-state diffusion welding [12], resistance spot welding [15], upset resistance welding (URW) [21] and explosive welding/annealing [16]. The formation of reaction product layers (intermetallics) in these systems influences both the electrical conductivity and mechanical strength of the composites. Prolonged annealing of Cu/Al ball bonds at 250 °C led to the formation of Cu_9Al_4 and $CuAl_2$ as the main intermetallic products [14].

In [21], URW was used for producing joints with high strength and electrical conductivity between aluminum and copper rods. This joining method utilizes electric current and mechanical pressure to form metallurgical bonds. Because of the imperfect contact between the workpieces to be joined, the electrical resistance at the interface (contact resistance) is high, which may lead to a temperature rise and melting of the metals during the current passage. The reaction layer at the interface was composed of cellular Al_2Cu and a lamellar eutectic structure composed of α-Al and Al_2Cu. It was found that an increase in the welding current and a decrease in the upset force result in an increase in the reaction layer thickness and strength of the joint.

In terms of the simultaneous application of pressure and electric current, spark plasma sintering (SPS) is similar to URW. SPS is widely used in laboratories and industry for the consolidation of powders and materials fabrication [22–24]. Consolidation of metals by SPS has an advantage of fast processing to high relative densities. Hot pressing (HP) is similar to SPS by the use of uniaxial pressure and consolidation of powders in a rigid die. The main difference between the HP and SPS methods is in the mode of heating: in the former, the external heating elements are used, while the electric current is passing directly through the conductive tooling and the conductive specimen in the latter. The electric current-assisted processing was used to form Cu-Al composites [15,21]. However, to the best of our knowledge, no comparative analysis of the behavior of the Cu-Al system under the SPS and HP conditions has been performed. In the SPS process, the intrinsic effect of electric current on the formation of the intermetallic products can be expected.

When consolidation of unalloyed powder blends is studied, the diffusion-related aspects need to be considered. If a powder blend is used for producing a composite by sintering, the diffusion processes between the metals play a major role in the structure and pore formation and shrinkage/swelling of the compact [25]. In a similar manner, pores can form upon annealing of layered structures. In the binary mixtures, if one metal diffuses faster into the other metal (alloy) of the diffusion couple during sintering, pores are formed in the locations of the former (Kirkendall effect) [26]. For the Cu-Al system, the Kirkendall effect was reported in several studies [27–29]. The faster diffusing element can be either copper or aluminum, depending on the stage of reaction advancement at the interface. Polyakova & Baimova [30] used molecular dynamic simulations to study the interdiffusion between Al and Cu under conditions of deformation close to those in high-pressure torsion. It was found that the character of the atomic mixing processes changes with the applied strain.

The goal of this investigation was to determine the influence of the consolidation/treatment method on the microstructure and phase composition of materials with non-equilibrium structures formed upon the partial reactive transformation of Cu-Al powder mixtures and layered systems. The formation of in situ composites during sintering of Cu-10 wt.% Al mixtures is described. The composites were obtained via SPS, HP and pressureless sintering. In Cu-Al mixtures, combustion reactions in the self-propagating and thermal explosion modes are possible with the use of pre-heating [31]; however, for the selected composition, the reaction proceeds gradually, as the concentration of Al is close to the combustion limit. A model experiment was conducted to better understand the interaction at the Cu/Al interface and the structural evolution of the diffusion couple. The intrinsic effect of electric current on the formation of reaction products was investigated using pre-deposited Cu/Al layers.

2. Materials and Methods

2.1. Starting Powder Materials

The starting materials were a copper powder (average particle size 40 μm, PMS-1 grade, 99.7%) and two aluminum powders differing in particle size, referred to below as fine and coarse (fine powder: 3–10 μm, PAD-6 grade, 99.9%; coarse powder: 10–45 μm, PA-4 grade, 98%). The SEM images of the Al and Cu powders are given in Figure 1. A

mixture of the Cu-10 wt.% Al composition was prepared by mixing in a mortar. The coarse Al powder was used for experiments described in Sections 3.2 and 3.3. The rest of the experiments on powder consolidation were conducted using a mixture containing the fine Al powder.

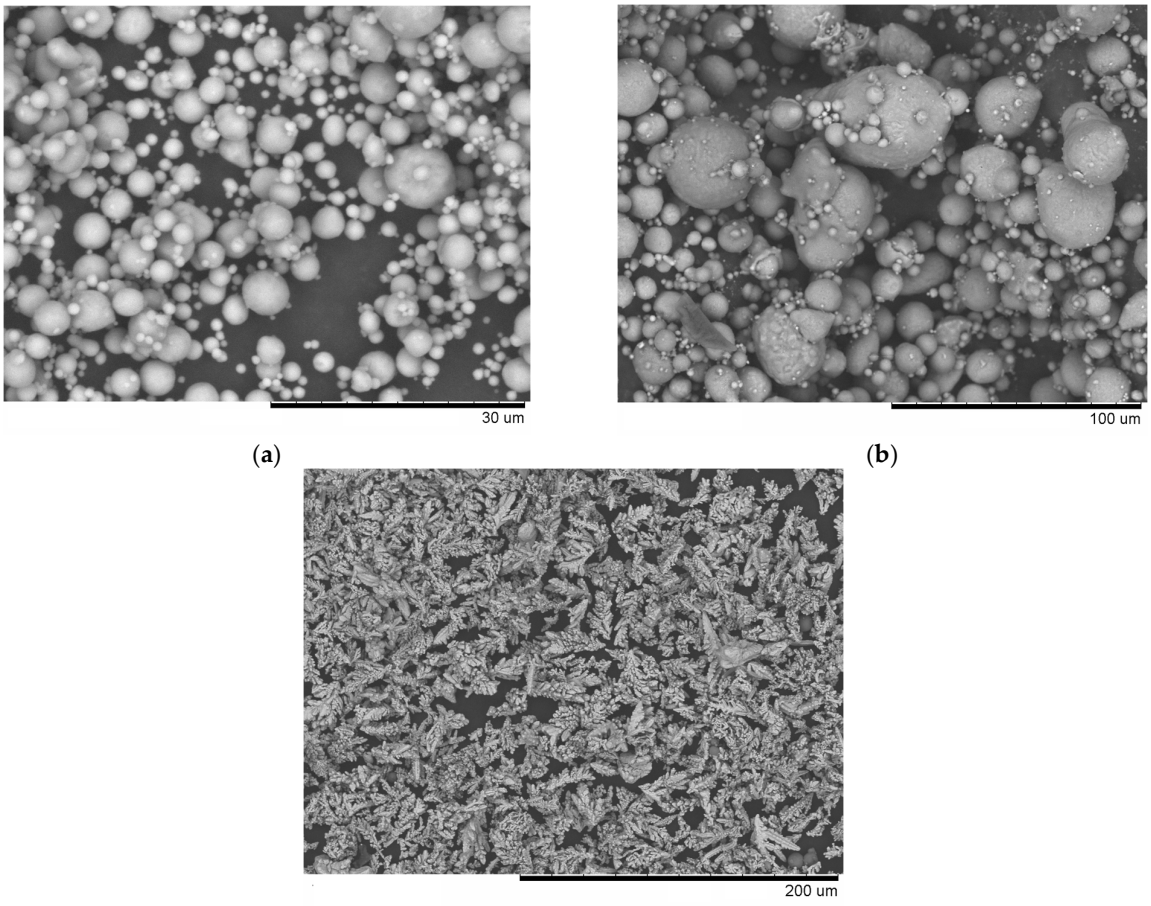

(**a**) (**b**)

(**c**)

Figure 1. Morphology of the starting Al and Cu powders: (**a**) Al, PAD-6 (fine powder), (**b**) Al, PA-4 (coarse powder) and (**c**) Cu, PMS-1.

2.2. Cold Pressing, Spark Plasma Sintering (SPS) and Hot Pressing (HP) of the Powders

Cold pressing of the Cu-10 wt.% Al mixture was conducted at room temperature at a pressure of 400 MPa in a steel die with a diameter of 10 mm. The relative density of the cold-pressed Cu-10 wt.% Al sample was 84%. The fine Al powder was used for preparing the mixture. The cold-pressed compacts were processed by SPS and pressureless sintering.

The SPS, HP and pressureless sintering experiments were performed at temperatures below the lowest eutectic in the Cu-Al system (548 °C) in order to study the solid-state sintering phenomena in the system.

A Labox 1575 apparatus (SINTER LAND Inc., Nagaoka, Japan) was utilized. Sintering was conducted under a uniaxial pressure of 40 MPa and dynamic vacuum. A graphite die with an inner diameter of 10 mm and an outer diameter of 40 mm and graphite punches were used. The temperature during the process was measured by a thermocouple inserted in a hole in the die wall. Sintering was conducted at 480 °C for 5 min.

For conducting HP, a facility developed by the Institute of Automation and Electrometry SB RAS, Novosibirsk, Russia, was used. HP was conducted in a graphite die with an inner diameter of 10 mm in an argon atmosphere at a uniaxial pressure of 40 MPa and a

temperature of 510 °C. The holding time at the maximum temperature was 5 min. The temperature during HP was measured by a pyrometer focused on the wall of the die.

The heating rate in the SPS and HP experiments was 60 °C min^{-1} and 50 °C min^{-1}, respectively.

The temperature of the HP experiments (510 °C) was set higher than the SPS temperature (measured by the thermocouple inserted in the die wall). This was done to make up for the difference in the real temperatures of the SPS and HP samples. In the low SPS temperature range, the real temperature of conductive samples is about 30–40 degrees higher than the measured temperature [32]. In the present work, additional experiments were conducted in the same SPS tooling, namely, heating of the Cu-50 vol.% Al (coarse powder) powder mixture above 480 °C at the same rate. At a measured temperature of 520 °C, the rapid punch displacement was observed, which indicated the formation of a liquid phase. This temperature is lower than the eutectic temperature in the Cu-Al system. Therefore, the measured temperature was ~30 degrees lower than the real temperature of the sample.

The accuracy of the temperature measurements during HP was confirmed by processing an Al powder. The compact was heated under a pressure of 40 MPa, and the rapid displacement of the punch was observed when a temperature of 660 °C (melting point of Al) was reached (according to the pyrometer reading).

The cold-pressed compact was sintered in a vacuum furnace at 510 °C for 5 min. The choice of the sintering temperature was dictated by the considerations given above for the comparative SPS and HP experiments. In the furnace, the sample was heated at a rate of 10 °C min^{-1}. After soaking at the maximum temperature, the sample was cooled down with the furnace.

2.3. A Model Experiment: Annealing of the Pre-Sintered Composite

A model diffusion experiment was conducted to trace the structural evolution of a sintered Cu-Al composite upon annealing. The Cu-10 wt.% Al composite was formed from the coarse Al powder by SPS at 480 °C and 40 MPa for 5 min and further annealed in the vacuum furnace at 510 °C for 1 h. The polished surface of the sample (the sample was polished prior to annealing) and the newly formed fracture surface of the annealed sample were investigated.

2.4. Formation of Cu/Al Layered Structures by Detonation Spraying and Treatment of the Layers by SPS and HP

For observing the intrinsic effect of electric current on the reactivity at the interface between the metals, Cu/Al layered structures were subjected to treatment by SPS and HP. The layered samples were fabricated by a computer-controlled detonation spraying set-up (CCDS2000, Novosibirsk, Russia) [33]. In detonation spraying, the powder particles are heated and accelerated by the products of detonation of oxygen–fuel mixtures. In the present work, the O_2/C_2H_2 molar ratio was 1.1. Nitrogen was used as a carrier gas. A layer of copper was first deposited on a steel substrate. Then, a layer of Al was deposited onto copper. The thickness of the Cu and Al layers was about 200 μm each. The use of detonation spraying allowed forming a layered structure of two metals bonded to each other with an interface free from reaction products.

Cylindrical samples 10 mm in diameter were machined from the plates to fit the SPS and HP tooling. The layered Cu/Al structures were treated by SPS at a measured temperature of 480 °C for 5 min and 20 min and by HP at 510 °C for 5 min. The applied pressure during SPS and HP was 40 MPa.

2.5. Structural Characterization of the Composite Materials and Hardness Measurements

The X-ray diffraction (XRD) patterns of the samples were recorded using a D8 ADVANCE diffractometer (Bruker AXS, Karlsruhe, Germany) with Cu Ka radiation. The quantitative analysis of the phase composition of the samples was performed in TOPAS

4.2 software (Bruker AXS, Karlsruhe, Germany). The phase contents determined from the XRD should be treated as a rough estimation only, as, in this method, the calculation error is usually several percent.

The microstructure of the sintered samples was studied on the polished cross-sections by scanning electron microscopy (SEM) using a TM-1000 Tabletop microscope (Hitachi, Tokyo, Japan). The back-scattered electron (BSE) imaging mode was used. The distribution of the elements in the layered samples was determined using a S-3400 N microscope working at 30 kV (Hitachi, Tokyo, Japan) and an energy-dispersive spectroscopy (EDS) unit (NORAN Spectral System 7, Thermo Fisher Scientific Inc., Waltham, MA, USA). The line and area modes of analysis were applied. The content of an Al-rich phase in the samples obtained by SPS was determined by analyzing the SEM images in ImageJ software (https://imagej.nih.gov, accessed on 1 June 2020). The contents were averaged from the analysis of 10 images of each sample. The images were taken at a magnification of ×1000.

The optical images of the samples were obtained on an OLYMPUS GX-51 metallographic microscope (Tokyo, Japan). The porosity of the composites, where possible, was determined from the optical images of the cross-sections of the samples using OLYMPUS Stream Image Analysis software "Stream Essentials 1.9.1" (Tokyo, Japan).

The Vickers hardness of the composites was measured by a DuraScan 50 tester (EMCO-TEST, Kuchl, Austria) at a load of 1 kg. An average value was determined from ten measurements and is reported together with the standard deviation.

3. Results and Discussion

3.1. Microstructure and Phase Composition of Composites Obtained by SPS and Pressureless Sintering of Cu-10 wt.% Al

Figure 2 shows the microstructure of the cold-pressed compact as well as those treated by SPS and sintered in the furnace without applying pressure. The structure of the unreacted mixture is shown in Figure 2a. The Al and Cu metals can be distinguished in both SEM and optical images. In the optical images, pure copper has a reddish color, while the Cu(Al) solid solutions are yellow. The Al and Cu_9Al_4 intermetallic regions are gray in the optical images. The microstructures of composites formed by SPS of the cold pressed compact and pressureless sintering of the same compact are different from each other (Figure 2b,c). The XRD phase analysis showed that the materials processed by SPS and pressureless sintering consisted of three phases: residual Cu, Cu_9Al_4 and Cu(Al) solid solution (Figure 3a,b). In the SPS-processed composite, the Cu_9Al_4 and Cu(Al) phases are present at close concentrations (Figure 3a, Table 1). In the composite obtained by pressureless sintering, the major phase (the matrix) is a solid solution (Figure 3b). The sintered material consists of 8 wt.% of Cu, 70 wt.% of Cu(Al) and 22 wt.% of Cu_9Al_4 (Table 1). A higher transformation degree in the sintered material is due to a longer total high-temperature exposure as compared with the SPS-processed composite (lower heating and cooling rates). At the same time, the sintered material remains porous, with a residual porosity of 23%. The relative density of this composite had to be determined for assessing its porosity, as it was not possible to directly determine the porosity from the optical images (the material obtained by pressureless sintering was soft and smeared during polishing). The shrinkage of the compact during pressureless sintering does occur, but it cannot compensate for the formation of porosity related to the difference in the diffusion fluxes of the metals. This porosity value is higher than that of the cold-pressed compact, which indicates the presence of porosity related to the Kirkendall effect (further details of this effect are given in Section 3.2).

Table 1. Phase contents estimated from the X-ray diffraction patterns, porosity and Vickers hardness of the in situ composites formed by consolidation of the Cu-10 wt.% Al mixtures. The holding time at the maximum temperature during SPS and pressureless sintering was 5 min. The measured temperature is given. The fine Al powder was used for the experiments.

Consolidation Conditions	Estimated Phase Contents, wt.%			Porosity, %	Vickers Hardness, HV_1
	Cu	Cu_9Al_4	Cu(Al)		
Cold pressing, pressuless sintering, 510 °C	8	22	70	23 *	90 ± 5
Cold pressing, SPS, 480 °C, 40 МПа	30	40	30	1.0 ± 0.3 **	250 ± 25
SPS of the mixture, 480 °C, 40 МПа	30	40	30	1.0 ± 0.3 **	205 ± 20

* calculated from the relative density (estimated from the precise measurements of the sample's dimensions and weight); the theoretical density is assumed to be 7.57 g cm^{-3}); ** determined from the optical images.

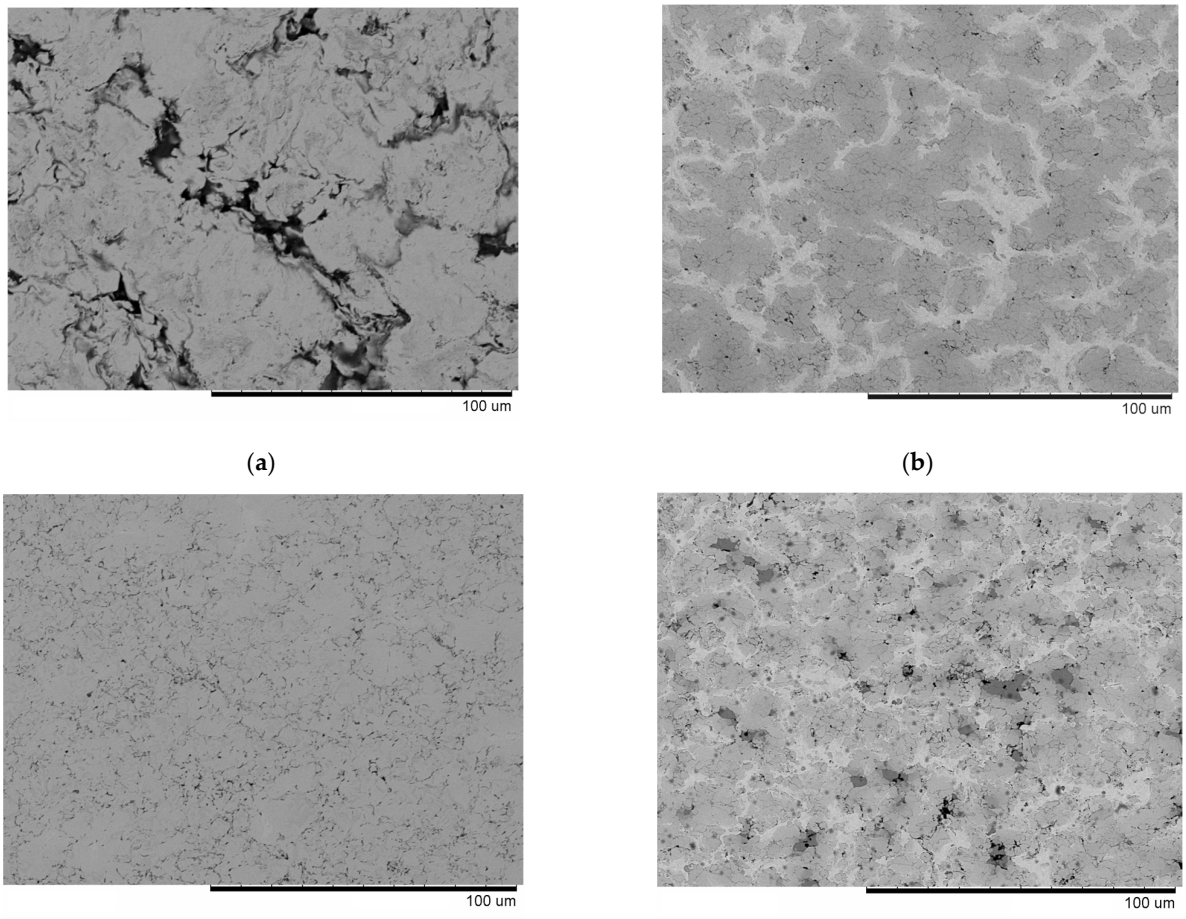

(**a**) (**b**)

(**c**) (**d**)

Figure 2. Microstructure of composites obtained from the Cu-10 wt.% Al powder mixture: (**a**) cold-pressed compact, (**b**) composite obtained by cold pressing followed by spark plasma sintering (SPS) at 480 °C, (**c**) composite obtained by cold-pressing followed by pressureless sintering at 510 °C, (**d**) composite obtained by SPS of the powder mixture at 480 °C. The fine Al powder was used for the experiments. See Section 2.2 for considerations on the temperature selection.

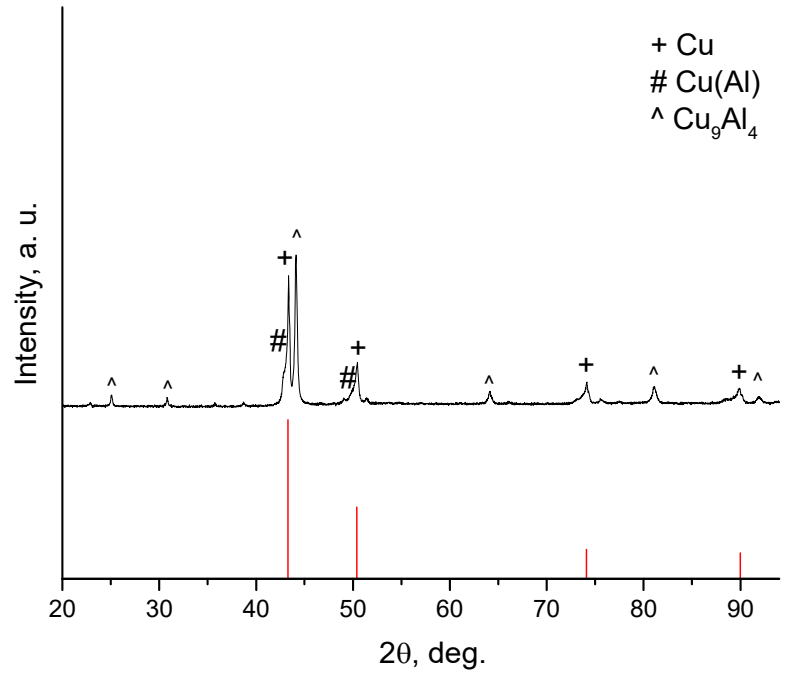

(**a**)

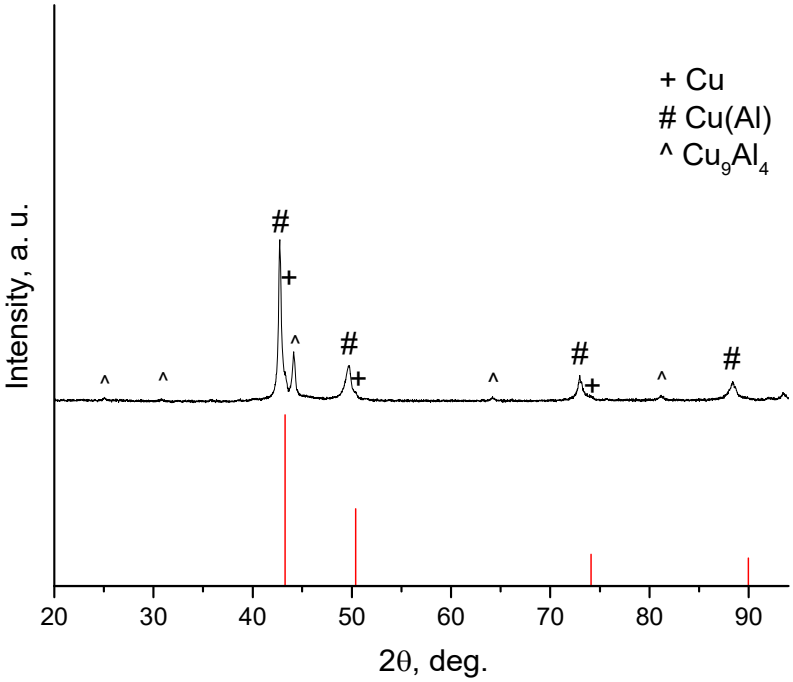

(**b**)

Figure 3. *Cont.*

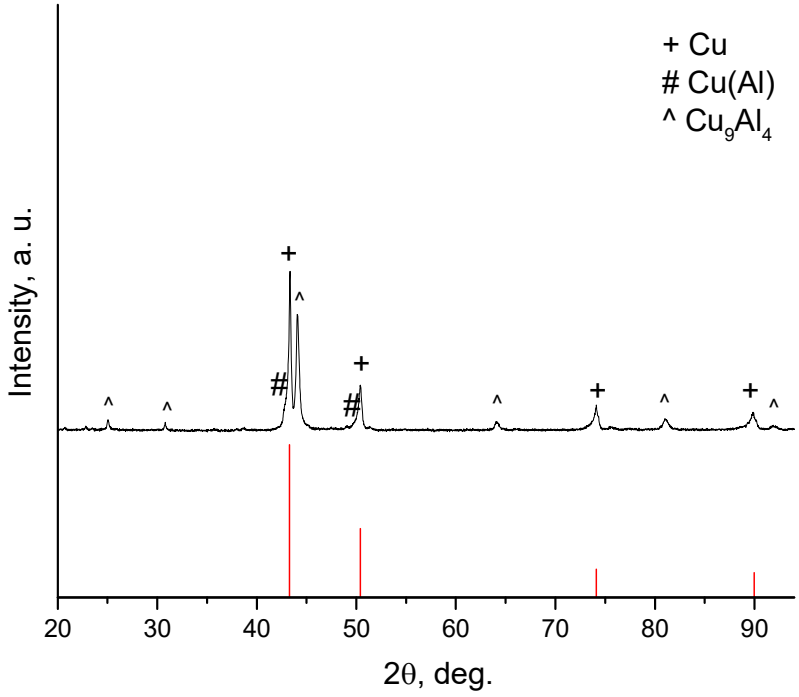

(**c**)

Figure 3. X-ray diffraction (XRD) patterns of composites obtained from the Cu-10 wt.% Al powder mixture: (**a**) cold pressing followed by SPS at 480 °C, (**b**) cold pressing followed by pressureless sintering at 510 °C, (**c**) SPS of the powder mixture at 480 °C. The fine Al powder was used for the experiments. The lines of copper (card #00-04-0836) are plotted in red.

In order to better understand the influence of the consolidation conditions on the synthesis outcome, the structures described above may be compared with that formed by direct SPS of the powder mixture. The XRD pattern of the material obtained by direct SPS of the powder mixture is given in Figure 3c. The estimated phase contents in the composites obtained by cold pressing/SPS and direct SPS of the powder mixture are close to each other (Table 1). The microstructure of the composite cold-pressed before SPS is characterized by a more advanced stage of interaction between the metals, as dark regions corresponding to an Al-rich phase ($CuAl_2$) seen in the images of Figure 2d are absent in Figure 2b. Although these regions are present in the microstructure of the sample obtained by direct SPS of the powder mixture, the $CuAl_2$ phase is difficult to detect by the XRD (the concentration of this phase is low). As estimated from the image analysis of the composites in ImageJ, the content of the phase corresponding to dark regions is only 5 vol.%.

The hardness of the composite formed by pressureless sintering is much lower than the hardness of composites formed by consolidation under pressure (Table 1) owing to a higher porosity of the former. The hardness of the composite formed by SPS of the cold-pressed compacts is slightly higher than the hardness of the composite formed directly from the powder mixture by SPS.

3.2. Kirkendall Effect in the Cu-Al System: A Model Experiment and Analysis of Diffusion Coefficients

In order to study the pore formation mechanism during pressureless sintering of Cu-Al composites, a compact formed by SPS was held at a temperature of 510 °C for 1 h. The coarse Al powder was taken for the experiments for an easy observation of pores in the locations of Al particles (in case of its full consumption). In the composite obtained by SPS, the Al particles only partially reacted with copper, forming core–shell structures. During

post-sintering annealing, the transformation degree of aluminum increased (Figure 4a). The fracture surface of the annealed compact demonstrating the formation of pores during annealing is shown in Figure 4b–d. The presence of bright particles within the volume of dark particles (Al) can be attributed to the formation of $CuAl_2$ precipitates due to diffusion of copper into aluminum. The character of distribution of these particles suggests the operation of grain boundary diffusion of copper in aluminum. Previously, the formation of fine $CuAl_2$ precipitates in an Al matrix in an (Al-Cu-Fe)-Al composite due to diffusion of copper from the alloy particles into aluminum was reported in [34]. In Figure 4b,c, the residual Al particles smaller in size than the pores are observed. In Figure 4d, an empty pore with walls formed by the reaction products between Cu and Al is shown.

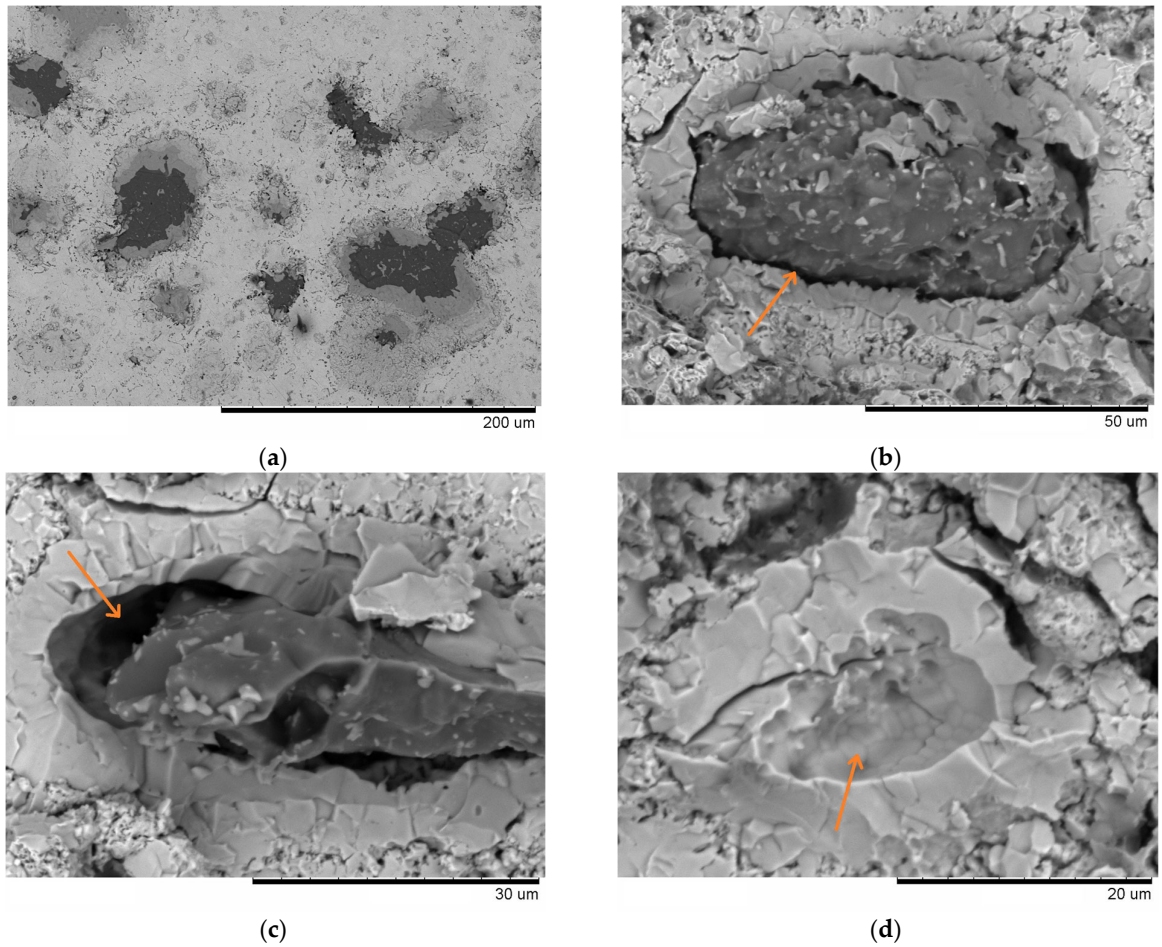

Figure 4. (**a**) SEM image of the compact consolidated by SPS at 480 °C and further annealed for 1 h at 510 °C. (**b**–**d**) Fracture surface of the annealed compact demonstrating the formation of pores. In (**b**,**c**), the residual Al particles are smaller in size than the pores and in some places (indicated by arrows) are separated from the walls of the pores. In (**d**), an empty pore (indicated by the arrow) with walls formed by the reaction products between Cu and Al is seen. The coarse Al powder was used.

The diffusion coefficients of the metals were calculated for a temperature of 500 °C. The diffusion coefficient of copper in aluminum $D_{Cu\ in\ Al}$ is 5×10^{-10} $cm^2\ s^{-1}$, while the diffusion coefficient of aluminum in copper $D_{Al\ in\ Cu}$ is 4×10^{-14} $cm^2\ s^{-1}$ (calculated based on [35]). Therefore, when a Cu/Al interface free of any reaction product is initially heated, copper atoms diffuse into aluminum. As the process advances, an intermetallic layer is formed to separate the metals. In the intermetallic layer or Al-rich solid solutions, the diffusion of Al atoms can be faster than that of Cu atoms. For example, in a solid solution containing 9 at.% of Al, $D_{Cu\ in\ Cu(Al)} = 9.8 \times 10^{-15}$ $cm^2\ s^{-1}$ and $D_{Al\ in\ Cu(Al)} = 1.3 \times 10^{-13}$ $cm^2\ s^{-1}$ [36]. So, once a layer of the intermetallic products sepa-

rating the initial metals has formed, it is the fast diffusion of aluminum atoms into copper that determines the further structural evolution of the system during annealing.

For the properties of the sintered Cu-10 wt.% Al alloy, the Kirkendall porosity is detrimental, so the powder mixture should be prepared and processed in such a way as to avoid the formation of large pores. The size of pores is comparable to the size of Al particles. Therefore, the use of fine Al powder and the application of pressure during consolidation can help solve the problem of the porosity caused by the Kirkendall effect.

3.3. The Influence of the Processing Method (SPS/HP) on the Interaction beween Cu and Al in Sintered Materials and Layered Structures

For observing the effect of the treatment method, SPS versus HP, on the growth of the reaction products between Cu and Al, experiments were conducted with a Cu-10 wt.% Al mixture containing the coarse Al powder. As seen in Figure 5a, after SPS, layers of reaction products surround the Al particles such that core–shell structures form. In the corresponding HP experiment, these layers are thinner or even absent around some particles (Figure 5b). A lower transformation degree in the HP experiment was also confirmed by the XRD analysis.

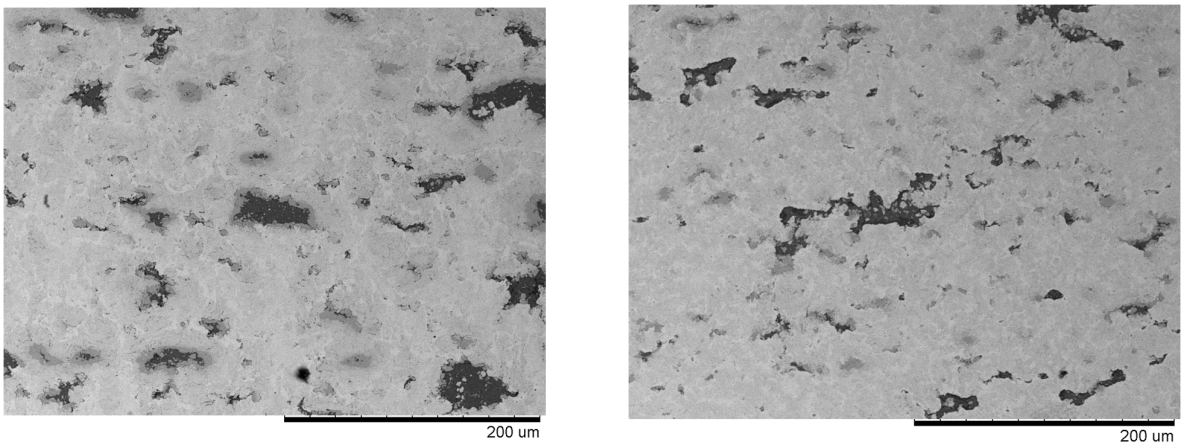

Figure 5. Microstructure of composites obtained from the Cu-10 wt.% Al powder mixture: (**a**) SPS, 480 °C (**b**) hot pressing (HP), 510 °C. The coarse Al powder was used for the experiments. See Section 2.2 for considerations on the temperature selection.

The experiments were also conducted on pre-deposited layers of Cu and Al. The layered structures were processed by SPS and HP. A SEM image of the cross-section of the Cu/Al layered structure obtained by detonation spraying is presented in Figure 6a. The layer of the reaction products at the Cu/Al interface is thinner in the case of HP treatment (Figure 6b) than in the case of SPS (Figure 6c), suggesting that the passing electric current facilitates the interaction between the metals. Here, the presence of any effects of local character (such as overheating due to high current densities at the poorly developed contacts) is excluded, as pre-deposited layers with a well-developed interface were used as a starting assembly for experiments.

In order to determine the composition of the products of interaction, a thicker layer was grown at the interface between the metals by soaking the layered structure for 20 min in the SPS set-up (Figure 6d). The results of the EDS line analysis of the interface are demonstrated in Figure 7. The Cu/Al ratio in the layers marked I (Al-rich) and II (Cu-rich) was determined using the area mode of EDS (the areas analyzed were within the layer). The Cu/Al atomic ratio was 35/65 and 63/37 in layers I and II, respectively. The ratio of the metals in layer I is close to that in the $CuAl_2$ compound, while the Cu/Al ratio in layer II is close to the metal ratio in Cu_9Al_4. By analyzing the contrast in the images shown in

Figure 6b,c, it can be concluded that, during the HP treatment, an Al-rich layer mainly formed. During SPS, a thicker Al-rich layer formed, and a Cu-rich layer also appeared.

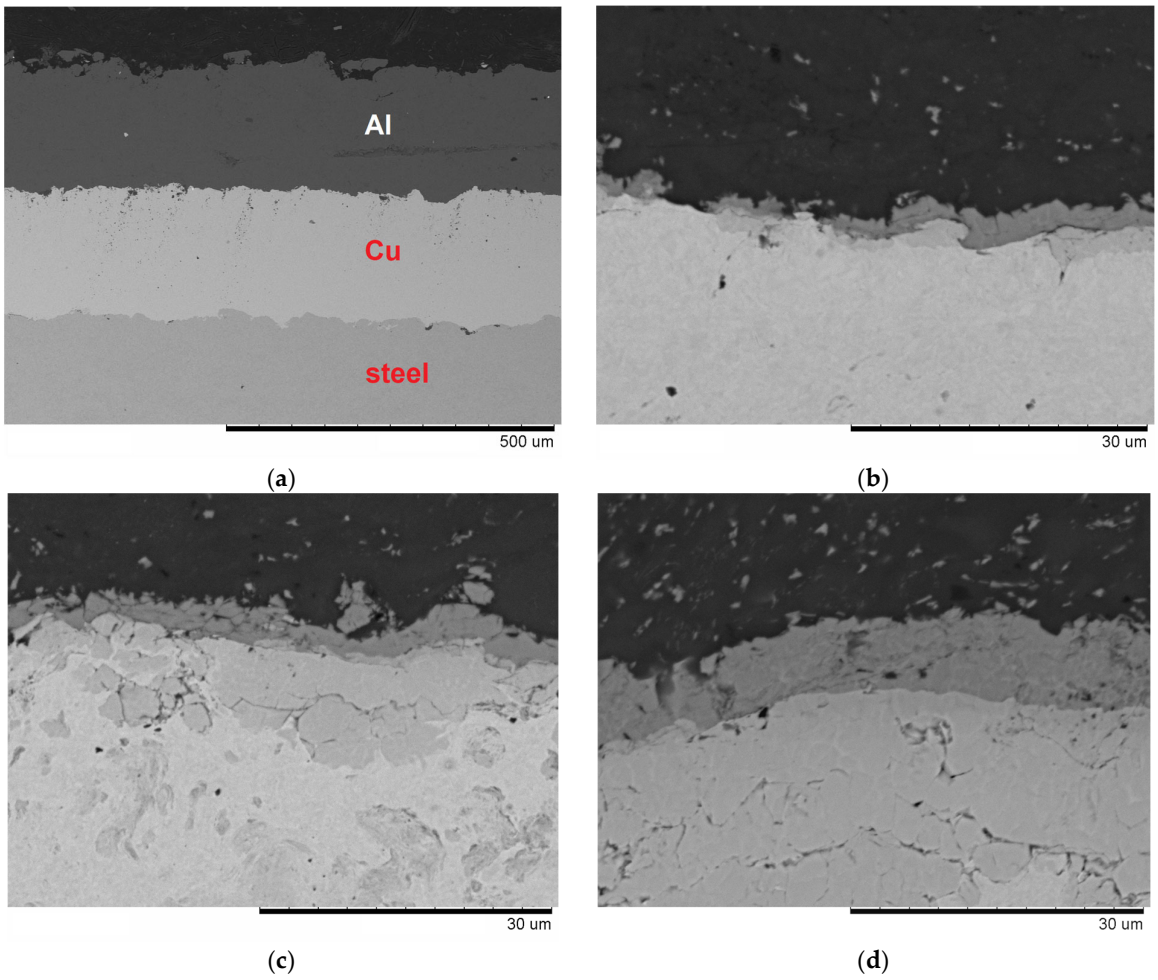

Figure 6. SEM images of the cross-section of the Cu/Al layered structure obtained by detonation spraying (**a**), after HP treatment at 510 °C for 5 min (**b**) and after SPS treatment at 480 °C for 5 min (**c**) and 20 min (**d**). See Section 2.2 for considerations on the temperature selection.

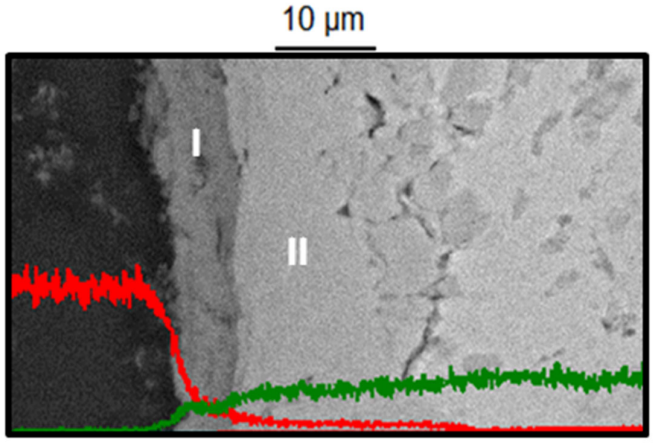

Figure 7. Energy-dispersive spectroscopy line analysis of the interface formed during the SPS treatment of the Cu/Al layered structure at 480 °C for 20 min. Red line—Al signal, green line—Cu signal. The Cu/Al ratio in the layers marked I and II was determined (I—Al-rich layer, II—Cu-rich layer).

The effect of current on systems of dissimilar metals may be related to the formation of thermal gradients across the interface, as elaborated in [37]. Previous studies of the effect of electric current on metallic systems (Ni-Al [38], Fe-Al [39], Ni-Ti [40]) showed the enhancement of the reactivity of the metals. Further research is required to determine the mechanisms of the influence of electric current on the reactivity of metals, including experiments with layered structures composed of a metal and a pre-synthesized intermetallic compound and those with alloys of different compositions.

4. Conclusions

In the present work, the interaction of copper and aluminum under different processing conditions at temperatures below the lowest melting point eutectic in the Cu-Al system was studied. The phase composition and microstructure of materials formed from Cu+Al mixtures depend on the consolidation conditions of the powders. Cold pressing of the mixture before SPS leads to a higher transformation degree of the metals during sintering. Pressureless sintering of the cold-pressed Cu-10 wt.% Al compact at 510 °C results in the formation of a porous material. The microstructural evidence of diffusion of Cu into Al and of Al into Cu was observed. During pressureless sintering at 510 °C, the predominant diffusion of Al atoms into copper through the reaction product layer led to the formation of pores in the locations of Al particles. The electric current passing through the Cu/Al interface facilitates the interaction between the metals. This effect was directly observed by inducing the interaction in the pre-deposited Cu/Al layers and a Cu-Al mixture containing a coarse Al powder (not fully reacted during the processing). Overall, in order to form materials with a low residual porosity in the Cu-10 wt.% Al system, pressure-assisted powder consolidation methods (HP, SPS) should be used. The acceleration of the intermetallic formation at Al/Cu interfaces by electric current is a feature of the SPS processing of composites with layered structure and composites reinforced with core–shell (Al core–intermetallic shell) particles. The results of studies of the formation mechanisms of Cu-Al materials by solid state sintering can be used in the development of composite conductors and bronzes with a non-equilibrium structure.

Author Contributions: Conceptualization, D.V.D. and B.B.B.; methodology, B.B.B., S.F.T. and V.Y.U.; investigation, A.V.U., O.L.S., A.I.G. and A.A.O.; writing—original draft preparation, D.V.D.; writing—review and editing, O.L.S. and S.F.T.; supervision, D.V.D.; project administration, D.V.D.; funding acquisition, V.Y.U. All authors have read and agreed to the published version of the manuscript.

Funding: The support from the Ministry of Science and Higher Education of the Russian Federation, project #121032500062-4 (ISSCM SB RAS) and project #121121600298-7 (LIH SB RAS), is gratefully acknowledged.

Institutional Review Board Statement: Not applicable.

Informed Consent Statement: Not applicable.

Data Availability Statement: Data can be made available upon request.

Acknowledgments: The authors are grateful to Vyacheslav V. Markushin for his help with the preparation of the metallographic samples of the composites.

Conflicts of Interest: The authors declare no conflict of interest. The funders had no role in the design of the study, in the collection, analyses or interpretation of the data, in the writing of the manuscript or in the decision to publish the results. The authors declare that the research was conducted in the absence of any commercial or financial relationships that could be construed as a potential conflict of interest.

References

1. Casati, R.; Vedani, M. Metal matrix composites reinforced by nano-particles—A review. *Metals* **2014**, *4*, 65–83. [CrossRef]
2. Dudina, D.V.; Georgarakis, K. Core–shell particle reinforcements—A new trend in the design and development of metal matrix composites. *Materials* **2022**, *15*, 2629. [CrossRef] [PubMed]

3. Schramm Deschamps, I.; dos Santos Avila, D.; Vanzuita Piazera, E.; Dudley Cruz, R.C.; Aguilar, C.; Klein, A.N. Design of in situ metal matrix composites produced by powder metallurgy—A critical review. *Metals* **2022**, *12*, 2073. [CrossRef]
4. Dudina, D.V.; Georgarakis, K.; Olevsky, E.A. Progress in aluminium and magnesium matrix composites obtained by spark plasma, microwave and induction sintering. *Int. Mater. Rev.* **2023**, *68*, 225–246. [CrossRef]
5. Heinz, A.; Haszler, A.; Keidel, C.; Moldenhauer, S.; Benedictus, R.; Miller, W.S. Recent development in aluminium alloys for aerospace applications. *Mater. Sci. Eng. A* **2000**, *280*, 102–107. [CrossRef]
6. Prados, E.F.; Sordi, V.I.; Ferrante, M. The effect of Al_2Cu precipitates on the microstructural evolution, tensile strength, ductility and work-hardening behaviour of a Al–4 wt.% Cu alloy processed by equal-channel angular pressing. *Acta Mater.* **2013**, *61*, 115–125. [CrossRef]
7. Zhai, W.; Lu, W.; Zhang, P.; Zhou, M.; Liu, X.; Zhou, L. Microstructure, mechanical and tribological properties of nickel-aluminium bronze alloys developed via gas atomization and spark plasma sintering. *Mater. Sci. Eng. A* **2017**, *707*, 325–336. [CrossRef]
8. Shaik, M.A.; Golla, B.R. Densification, microstructure and properties of mechanically alloyed and hot-pressed Cu–15 wt% Al alloy. *J. Mater. Sci.* **2018**, *53*, 14694–14712. [CrossRef]
9. Shaik, M.A.; Golla, B.R. Development of highly wear resistant Cu–Al alloys processed via powder metallurgy. *Tribol. Int.* **2019**, *136*, 127–139. [CrossRef]
10. Chesnokov, A.E.; Kosarev, V.F.; Klinkov, S.V.; Smirnov, A.V.; Vidyuk, T.M. Influence of mechanical milling and Heat Treatment on the properties of bronze powder. *Inorganic Mater.* **2021**, *57*, 249–254. [CrossRef]
11. Ondar, A.A.; Dudina, D.V.; Grigoreva, T.F.; Devyatkina, E.T.; Vosmerikov, S.V.; Ukhina, A.V.; Esikov, M.A.; Anisimov, A.G.; Lyakhov, N.Z. Cu–10 wt.% Al alloys produced by spark plasma sintering of powder blends and a mechanically alloyed mixture: A comparative investigation. *Powders* **2023**, *2*, 515–524. [CrossRef]
12. Bedjaoui, W.; Boumerzoug, Z.; Delaunois, F. Solid-state diffusion welding of commercial aluminum alloy with pure copper. *Int. J. Autom. Mech. Eng.* **2022**, *19*, 9734–9746. [CrossRef]
13. Mulyukov, R.R.; Korznikova, G.F.; Nazarov, K.S.; Khisamov, R.K.; Sergeev, S.N.; Shayachmetov, R.U.; Khalikova, G.R.; Korznikova, E.A. Annealing induced phase transformations and hardness evolution in Al–Cu–Al composites obtained by high-pressure torsion. *Acta Mech.* **2021**, *232*, 1815–1828. [CrossRef]
14. Hang, C.J.; Wang, C.Q.; Mayer, M.; Tian, Y.H.; Zhou, Y.; Wang, H.H. Growth behavior of Cu/Al intermetallic compounds and cracks in copper ball bonds during isothermal aging. *Microelectron. Reliab.* **2008**, *48*, 416–424. [CrossRef]
15. Zare, M.; Pouranvari, M. Metallurgical joining of aluminium and copper using resistance spot welding: Microstructure and mechanical properties. *Sci. Technol. Weld. Join.* **2021**, *26*, 461–469. [CrossRef]
16. Shiran, M.K.G.; Khalaj, G.; Pouraliakbar, H.; Jandaghi, M.R.; Dehnavi, A.S.; Bakhtiari, H. Multilayer Cu/Al/Cu explosive welded joints: Characterizing heat treatment effect on the interface microstructure and mechanical properties. *J. Manuf. Process.* **2018**, *35*, 657–663. [CrossRef]
17. Abbasi, M.; Karimi Taheri, A.; Salehi, M.T. Growth rate of intermetallic compounds in Al/Cu bimetal produced by cold roll welding process. *J. Alloys Compd.* **2001**, *319*, 233–241. [CrossRef]
18. Li, L.; Deng, G.; Zhai, W.; Li, S.; Gao, X.; Wang, T. The growth of intermetallic compounds and its effect on bonding properties of Cu/Al clad plates by CFR. *Metals* **2022**, *12*, 1995. [CrossRef]
19. Li, Q.; Zhang, Y.; Cheng, Y.; Zuo, X.; Wang, Y.; Yuan, X.; Huang, H. Effect of temperature on the corrosion behavior and corrosion resistance of copper–aluminum laminated composite plate. *Materials* **2022**, *15*, 1621. [CrossRef]
20. Cheng, Y.; Yuan, X.; Huang, H.; Zuo, X.; Zhang, Y. Salt-spray corrosion behavior of a Cu–Al composite plate under AC current. *Mater. Corros.* **2020**, *71*, 608–616. [CrossRef]
21. Shamsian, M.; Movahedi, M.; Kokabi, A.H.; Ozlati, A. Upset resistance welding of aluminium to copper rods: Effect of interface on performance. *Mater. Sci. Technol.* **2018**, *34*, 1830–1838. [CrossRef]
22. Tokita, M. Progress of spark plasma sintering (SPS) method, systems, ceramics applications and industrialization. *Ceramics* **2021**, *4*, 160–198. [CrossRef]
23. Monchoux, J.P.; Couret, A.; Durand, L.; Voisin, T.; Trzaska, Z.; Thomas, M. Elaboration of metallic materials by SPS: Processing, microstructures, properties, and shaping. *Metals* **2021**, *11*, 322. [CrossRef]
24. Abedi, M.; Sovizi, S.; Azarniya, A.; Giuntini, D.; Seraji, M.E.; Hosseini, H.R.M.; Amutha, C.; Ramakrishna, S.; Mukasyan, A. An analytical review on Spark Plasma Sintering of metals and alloys: From processing window, phase transformation, and property perspective. *Crit. Rev. Solid State Mater. Sci.* **2023**, *48*, 169–214. [CrossRef]
25. German, R.M. *Sintering: From Empirical Observations to Scientific Principles*; Butterworth-Heinemann: Oxford, UK, 2014; 544p.
26. Dudina, D.V.; Kvashnin, V.I.; Matvienko, A.A.; Sidelnikov, A.A.; Gavrilov, A.I.; Ukhina, A.V.; Moreira Jorge, A., Jr.; Georgarakis, K. Towards a better understanding of the interaction of $Fe_{66}Cr_{10}Nb_5B_{19}$ metallic glass with aluminum: Growth of intermetallics and formation of Kirkendall porosity during sintering. *Chemistry* **2023**, *5*, 138–150. [CrossRef]
27. Yadav, D.; Bauri, R. Development of Cu particles and Cu core-shell particles reinforced Al composite. *Mater. Sci. Technol.* **2015**, *31*, 494–500. [CrossRef]
28. Savitskii, K.V.; Itin, V.I.; Kozlov, Y.I. The mechanism of sintering of copper-aluminum powder alloys in the presence of a liquid phase. *Sov. Powder Metall. Metal Ceram.* **1966**, *5*, 4–9. [CrossRef]
29. Liu, W.; Cui, J.Z. The Kirkendall effect of the Al-Cu couple with an electric field. *J. Mater. Sci. Lett.* **1997**, *16*, 930–932. [CrossRef]

30. Polyakova, P.V.; Baimova, J.A. The effect of atomic interdiffusion at the Al/Cu interface in an Al/Cu composite on its mechanical Properties: Molecular dynamics. *Phys. Metals Metallogr.* **2023**, *124*, 394–401. [CrossRef]
31. Itin, V.I.; Bratchikov, A.D.; Postnikova, L.N. Use of combustion and thermal explosion for the synthesis of intermetallic compounds and their alloys. *Sov. Powder Metall. Metal Ceram.* **1980**, *19*, 315–318. [CrossRef]
32. Kvashnin, V.I.; Dudina, D.V.; Ukhina, A.V.; Koga, G.Y.; Georgarakis, K. The benefit of the glassy state of reinforcing particles for the densification of aluminum matrix composites. *J. Compos. Sci.* **2022**, *6*, 135. [CrossRef]
33. Ulianitsky, V.Y.; Dudina, D.V.; Shtertser, A.A.; Smurov, I. Computer-controlled detonation spraying: Flexible control of the coating chemistry and microstructure. *Metals* **2019**, *9*, 1244. [CrossRef]
34. Joseph, A.; Gauthier-Brunet, V.; Joulain, A.; Bonneville, J.; Dubois, S.; Monchoux, J.-P.; Pailloux, F. Mechanical properties of Al/ω–Al–Cu–Fe composites synthesized by the SPS technique. *Mater. Charact.* **2018**, *145*, 644–652. [CrossRef]
35. Neumann, G.; Tuijn, C. *Self-Diffusion and Impurity Diffusion in Pure Metals: Handbook of Experimental Data*; Pergamon: Oxford, UK, 2009; 349p.
36. Oikawa, H.; Karashima, S. On the self-diffusion coefficients of aluminum in copper (rich)-aluminum solid solutions. *Trans. Japan. Inst. Metals* **1970**, *11*, 431–433. [CrossRef]
37. Rudinsky, S.; Gauvin, R.; Brochu, M. The effects of applied current on one-dimensional interdiffusion between copper and nickel in spark plasma sintering. *J. Appl. Phys.* **2014**, *116*, 154901. [CrossRef]
38. Abedi, M.; Asadi, A.; Sovizi, S.; Moskovskikh, D.; Vorotilo, S.; Mukasyan, A. Influence of pulsed direct current on the growth rate of intermetallic phases in the Ni–Al system during reactive spark plasma sintering. *Scr. Mater.* **2022**, *216*, 114759. [CrossRef]
39. Li, R.; Yuan, T.; Liu, X.; Zhou, K. Enhanced atomic diffusion of Fe–Al diffusion couple during spark plasma sintering. *Scr. Mater.* **2016**, *110*, 105–108. [CrossRef]
40. Garay, J.E.; Anselmi-Tamburini, U.; Munir, Z.A. Enhanced growth of intermetallic phases in the Ni–Ti system by current effects. *Acta Mater.* **2003**, *51*, 4487–4495. [CrossRef]

Disclaimer/Publisher's Note: The statements, opinions and data contained in all publications are solely those of the individual author(s) and contributor(s) and not of MDPI and/or the editor(s). MDPI and/or the editor(s) disclaim responsibility for any injury to people or property resulting from any ideas, methods, instructions or products referred to in the content.